Structural, Mössbauer and Raman studies of the $(Y,Ce)_2Sr_2Cu_2FeO_{8+y}$ compound

M. Pissas,* G. Kallias, N. Poulakis, D. Niarchos, and A. Simopoulos
Institute of Materials Science, National Centre for Scientific Research Demokritos, 153 10 Agia Paraskevi, Attiki, Greece

E. Liarokapis
Department of Physics, National Technical University of Athens, 157 80 Athens, Greece
(Received 3 February 1995; revised manuscript received 10 May 1995)

The crystal structure and physical properties for $(Y,Ce)_2Sr_2Cu_2FeO_{8+y}$ compound are reported using Rietveld refinement of x-ray powder-diffraction data, dc magnetic susceptibility, Mössbauer, and Raman spectroscopy measurements. Mössbauer data can be analyzed with three components. Component A is attributed to Fe^{3+} ($S = 5/2$) ions in the Cu(2) site. Component B is attributed to Fe^{3+} ($S = 3/2$) ions in the Cu(1) plane and appears only in the oxygen saturated sample. For the reduced sample, component B transforms to component D_r, which has a lower oxygen coordination number with respect to that of component B. The Raman lines are assigned to definite atomic vibrations in close comparison with other compounds of similar structure.

I. INTRODUCTION

Since the discovery of superconductivity in the $La_{2-x}Ba_xCuO_{4+y}$ oxide[1] various kinds of cuprate superconductors have been discovered. The basic structure of cuprate superconductors may be regarded as a layered structure consisting of CuO_2 sheets and interning slabs of Bi_2O_2, SrO, Y, (Pb,Cu)O, Tl_2O_3, and HgO. As a consequence new compounds can be easily designed by the replacement of a certain slab with another. In this context the homologous series $(Fe,Cu)Sr_2(Y,Ce)_nCu_2O_{4+2n+y}$ ($12n2$) have been synthesized from Wada *et al.*[2] Their structure can be obtained from that of the 123 compound by replacing the rare-earth layer with a fluorite structured layer, while substituting Sr for Ba. The $n = 2$ member (which is the subject of this paper), for brevity called 1222, is derived from the $CuSr_2YCu_2O_{6+y}$ (1212) by simultaneous substitution of the CuO layer with an (Fe,Cu)O layer and of the Y layer with a fluoritelike $(Y,Ce)_2O_2$ lamella. The substitution of the Y layer for the fluoritelike lamella has only minor structural effects elsewhere in the structure. The fluorite block increases the thickness of the neighboring perovskite block and usually has negative charge. So, it acts as an electron donor $\{[(Y^{3+},Ce^{4+})O_2^{-2}]^{\delta-}\}$ and since the perovskite block accepts the electrons from the fluorite block, the hole concentration in the CuO_2 planes decreases. In order to stabilize the 1212 and 1222 phases a high oxygen pressure is needed during the preparation procedure. However, if part of Cu is substituted for Fe the above compounds can be stabilized under atmospheric pressure. In the same family belongs also the $(Y,Ce)_2Sr_2CuFeO_8$. Its difference with 1222 is the absence of the oxygen deficient Cu(1) planes. In this compound the simultaneous presence of Cu and Fe with ratio 1:1 is needed in order to obtain stabilization.[3] We can include this compound in common with the $12n2$ family if instead of the formula $12n2$ we use the formula $m2n2$ for $m = 0$, $n = 2$.

In this paper we report a structural and lattice vibrations study of the $Y_{1.5}Ce_{0.5}Sr_2Cu_2FeO_{8+y}$ compound by means of the Rietveld analysis of x-ray powder-diffraction data and Raman spectroscopy. Magnetic-susceptibility measurements and ^{57}Fe Mössbauer spectroscopy were used to study the distribution of Fe among the Cu(1) and Cu(2) sites as well as the valence and the magnetic properties of iron in oxygen rich and oxygen reduced samples. The correlation of the results for the $(Y,Ce)_2Sr_2Cu_2FeO_{8+y}$ compound is discussed with respect to the $YSr_2Cu_{3-x}Fe_xO_y$ compounds.

II. EXPERIMENTAL DETAILS

Samples with nominal composition $Y_{2-z}Ce_zSr_2Cu_2FeO_{8+y}$ with $z = 0$, 0.25, 0.5, and 1.25 were prepared by thoroughly mixing high-purity stoichiometric amounts of Y_2O_3, CeO_2, $SrCO_3$, CuO, and Fe_2O_3. The mixed powders were pelletized and annealed in air at 1070 °C for 24 h. After an intermediate grinding the samples were annealed at 1120 °C for 6 days and finally they were quenched at room temperature (RT). The as-prepared samples were post annealed at 500 °C under flowing O_2. A subsequent furnace cooling under flowing O_2 was allowed (*oxygen saturated sample*, OS). Finally, a part of the as-prepared samples were post annealed at 500 °C under flowing Ar for one day and subsequently furnace cooled under flowing Ar (*oxygen reduced sample*, OR).

The above preparation route yields single phase materials only for $z = 0.5$. Any significant deviation from the above value of z leads to multiphase samples. For example for $z = 0$ and $z = 0.25$ we get 1212 as the major phase with Y_2O_3 ($z = 0$) and $(Ce,Y)O_2$ ($z = 0.25$) as

impurities. For $z = 1.25$ the x-ray-diffraction pattern revealed the coexistence of the $n = 2$ and $n = 3$ members as well as other extra diffraction peaks.

Thermogravimetric measurements were performed in a thermogravimetric analyzer (TGA) (Perkin Elmer TGS-2) by heating small amounts of sample up to 900 °C at a rate of 5 °C/min under the flow of 80% Ar+20% N_2. The x-ray-diffraction patterns were taken in the Bragg-Brentano geometry (from 20° to 120° with a step of 0.03°) with Cu $K\alpha$ radiation using a graphite crystal monochromator (Siemens D500).

Mössbauer spectra were taken using a conventional constant acceleration spectrometer with a ^{57}Co(Rh) source moving at RT, while the absorber was kept fixed at suitable temperatures. The spectra at temperatures higher than room temperature were taken in a furnace and the temperature stability was within 0.1 K. Velocity scale calibration was obtained by the room-temperature measurement of the spectra of an α−Fe foil.

Dc magnetization measurements were performed in a superconducting quantum interference device magnetometer (Quantum Design). The polarized Raman spectra were measured at room temperature using a triple spectrometer equipped with a microscope (Jobin-Ivon T64000) and a liquid-nitrogen-cooled CCD detector. An objective of 100× magnification was used both for focusing the laser beam ($\lambda = 514.5$ nm) and for collecting the scattered light. The laser power at the focus (1–2 μm diameter of the spot) was kept below 0.2 mW in order to avoid overheating.

III. THERMOGRAVIMETRY

Figure 1 shows the TGA trace of the OS sample. The sample starts to lose oxygen near 380 °C while a change in the slope of the weight loss vs temperature curve occurs near 600 °C. The temperature at which the weight loss starts is considerably higher than that of $YSr_2Cu_2FeO_y$ (135 °C),[4] while it is nearly equal to that of $Pr_{1.5}Ce_{0.5}Sr_2Cu_2Nb_{0.95}Fe_{0.05}O_{10}$ (380 °C) (Ref. 5) and $YBa_2Cu_{2.8}Fe_{0.2}O_{6+y}$ (350 °C).[6]

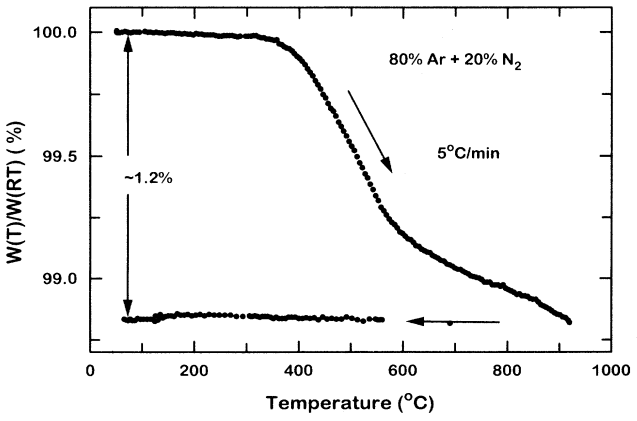

FIG. 1. The TGA trace for the OS $Y_{1.5}Ce_{0.5}Sr_2Cu_2FeO_{8+y}$ sample. The sample was heated under flowing Ar 80%+20% N_2 at a rate of 5 °C/min.

The overall weight loss of the sample is about 1.2%. Since the two oxygen atoms occupying the O(1) site represent the 4.5% of the unit formula weight, we conclude that the system loses about 0.5 oxygen atoms per formula unit. Approximately the same amount of oxygen loss per formula unit occurs in oxygen saturated $YSr_2Cu_2FeO_y$ and $YBa_2Cu_{2.3}Fe_{0.7}O_{6+y}$, e.g., 0.7 oxygen atoms for the first[4] and 0.73 for the second.[7] We also note that the oxygen loss in the compound under study is lower than in $YBa_2Cu_3O_7$ where the oxygen loss is nearly one oxygen per formula unit. The reason is that Fe-doped 1222 and Fe-doped Sr- and Ba-123 contain a large amount of iron at Cu(1) sites which due to its higher oxidation state holds the surrounding oxygen atoms, preventing them from escaping from the lattice during the heating in an inert atmosphere.

IV. STRUCTURAL STUDY

The structure of the $(Y,Ce)_2Sr_2Cu_2\ FeO_{8+y}$ compound is shown in Fig. 2 and consists of successive blocks with perovskitelike and calcium fluoritelike structure. The

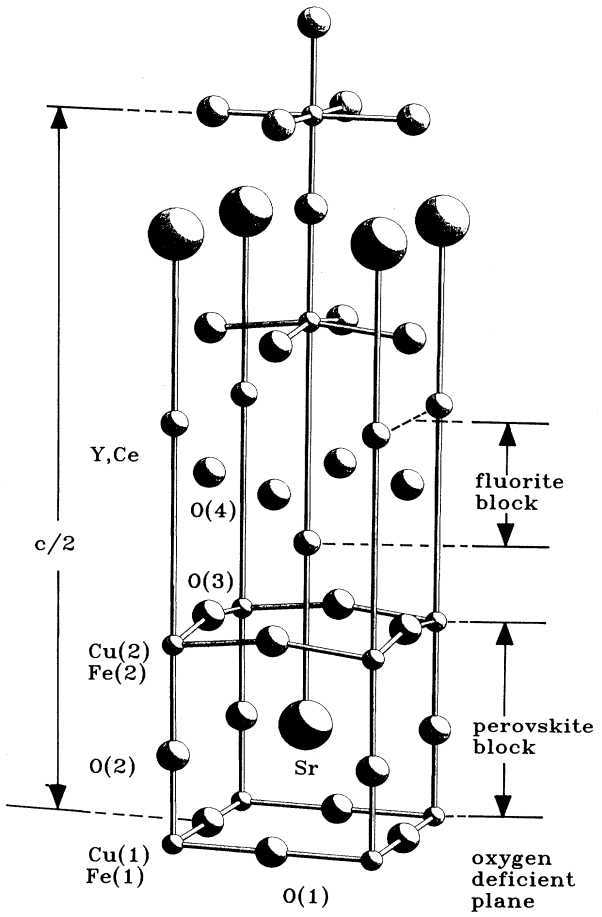

FIG. 2. Crystal structure of $(Y,Ce)_2Sr_2Cu_2FeO_{8+y}$.

layer sequence in the perovskite block, which is nearly 8 Å thick, can be represented as $Cu(2)O_2$-SrO-$Cu(1)O_y$-SrO-$Cu(2)O_2$. The perovskite blocks are separated by a block with calcium fluorite structure and thickness ≈ 6 Å, consisting of three layers [(Y,Ce)-O_2-(Y,Ce)]. Two successive blocks form a unit lamella with thickness ≈ 14 Å. The unit cell thus contains two unit lamella, related by a vector $1/2[111]_p$ (subscripts p refer to the unit cell with lattice parameter $a_p \times a_p \times c_p$, $a_p \approx 3.8$ Å, $c_p \approx 2 \times 14 = 28$ Å). The resulting structure has a body-centered lattice.

Rietveld profile refinements were carried out for both OS and OR samples in the $I4/mmm$ space group by using the BBWS-9006 Rietveld analysis program.[8] The profile shape function was assumed to be Pearson VII with $m = 1.1$ (Lorentzian function). Two different values of the isotropic thermal parameter B were assumed: one for all the cations and one for the oxygen atoms. The occupancy of the O(1) site was refined also. For the OS sample there are ≈ 9 oxygen atoms per formula unit, while for the OR sample there are ≈ 8.2 oxygen atoms per formula unit. This difference of 0.8 oxygen atoms is in good agreement with the thermogravimetry results. All species occupying the same site were constrained to have the same atomic positions (e.g., Y, Ce). The refinement showed that Ce shares with Y the site with the fluorite structure. Also, no disordering of the Ce and Sr cations was detected. Because of the similarity of the x-ray scattering factors of Fe and Cu we certainly cannot give a conclusive answer about the distribution of Fe among the two copper sites. Therefore, utilizing the results of the Mössbauer analysis (*vide infra*), we have assumed that Fe is equally distributed between the Cu(1) and Cu(2) sites.

Figure 3 shows a portion of the Rietveld refinement profile for the oxygenated sample. The pattern of the OR sample is similar (not shown). The refined parameters are listed in Table I while the calculated cation-oxygen bond lengths together with the calculated bond valence sums are listed in Table II. The bond valence sums were calculated using the relation $V_i = \sum_j \exp[(R_o - R_{ij})/B_o]$ where R_o is a constant dependent on the assumed valence state of the central ion and $B_o = 0.37$. The values of R_o for Cu^{+2}-O^{-2}, Sr^{+2}-O^{-2}, and Y^{+3}-O^{-2} were taken from Ref. 9. For Cu(1) and Sr the bond valence sums were calculated with the number of neighbors corrected for the fractional occupancy of the O(1) site (see Table II). The lattice parameters a and c increase upon removing

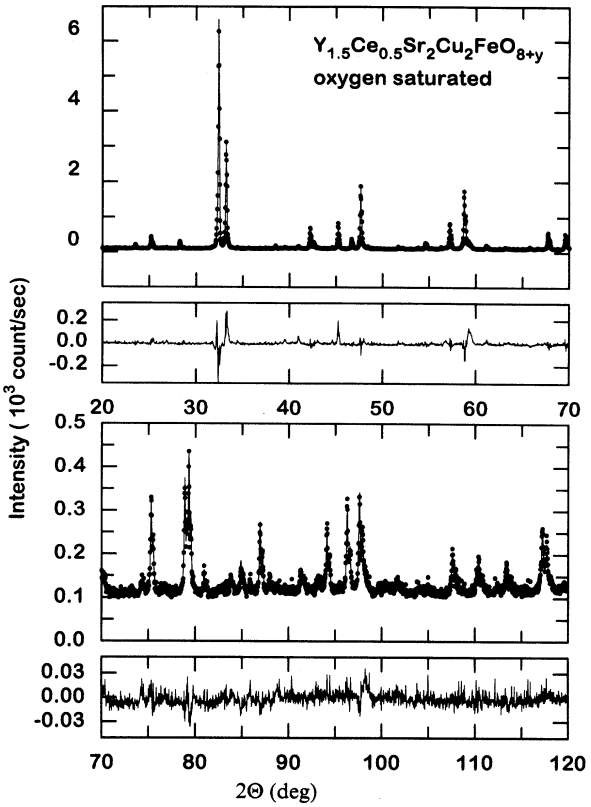

FIG. 3. Rietveld refinement patterns for the OS $Y_{1.5}Ce_{0.5}Sr_2Cu_2FeO_{8+y}$ sample. The observed intensities are shown with dots and the calculated ones by the solid line. The line in the bottom indicates the intensity difference between the experimental and the refined pattern.

TABLE I. Crystallographic data for the OS and OR $Y_{1.5}Ce_{0.5}Sr_2Cu_2FeO_{8+y}$ samples. Rietveld refinements were done in the $I4/mmm$ space group ($Z = 2$). $a = 3.8186(1)$ Å, $c = 28.0749(6)$ Å, $R_p = 7.3\%$, $R_{wp} = 8.2\%$, and $R_B = 8.8\%$ for the OS sample and $a = 3.8315(1)$ Å, $c = 28.2918(5)$ Å, $R_p = 6.2\%$, $R_{wp} = 6.8\%$, and $R_B = 8.9\%$ for the OR sample. The numbers in parentheses are estimated standard deviations referred to the last significant digit.

Atom	Wyckoff notation	x	y	z(OS)	z(OR)	B(OS)	B(OR)	N(OS)	N(OR)
Sr	4*e*	$\frac{1}{2}$	$\frac{1}{2}$	0.0741(1)	0.0802(1)	1.18(3)	0.63(2)	1.0	1.0
Y	4*e*	0	0	0.2959(1)	0.2952(1)	1.18(3)	0.63(2)	0.75	0.75
Ce	4*e*	0	0	0.2959(1)	0.2952(1)	1.18(3)	0.63(2)	0.25	0.25
Cu(1)	2*a*	0	0	0.0	0.0	1.18(3)	0.63(2)	1.0	1.0
Cu(2)	4*e*	0	0	0.1420(2)	0.1425(2)	1.18(3)	0.63(2)	1.0	1.0
O(1)	4*c*	0	$\frac{1}{2}$	0	0.0	2.3(2)	1.5(1)	0.5(1)	0.1(1)
O(2)	4*e*	0	0	0.0700(8)	0.0677(5)	2.3(2)	1.5(1)	1.0	1.0
O(3)	8*g*	$\frac{1}{2}$	0	0.1491(5)	0.1469(5)	2.3(2)	1.5(1)	1.0	1.0
O(4)	4*d*	$\frac{1}{2}$	0	$\frac{1}{4}$	$\frac{1}{4}$	2.3(2)	1.5(1)	1.0	1.0

TABLE II. Bond distances (Å) and bond valence sums V for the OS and OR $Y_{1.5}Ce_{0.5}Sr_2Cu_2FeO_{8+y}$ samples.

		Oxygen saturated	Oxygen reduced
Sr-O(2)	4×	2.702(1) Å	2.732(1) Å
Sr-O(1)	4×	2.823(2) Å	2.969(2) Å
Sr-O(3)	4×	2.84(1) Å	2.68(1) Å
V(Sr)		1.69(2)	1.71(3)
Y-O(4)	4×	2.303(1) Å	2.303(1) Å
Y-O(3)	4×	2.455(9) Å	2.520(9) Å
V(Y)		3.07(6)	2.89(6)
Cu(1)-O(1)	4×	1.909 Å	1.916 Å
Cu(1)-O(2)	2×	1.96(2) Å	1.91(1) Å
V[Cu(1)]		1.99(5)	1.58(5)
Cu(2)-O(3)	4×	1.919(1) Å	1.919(1) Å
Cu(2)-O(2)	1×	2.02(2) Å	2.11(1) Å
V[Cu(2)]		2.48(3)	2.39(2)

oxygen as in Ba- and Sr-123.

Regardless of the oxygen content, the apical distance Cu(1)-O(2) is $\approx$ 0.1 Å larger than in Ba- and Sr-123, while the Cu(2)-O(2) distance is $\approx$ 0.3 Å smaller than in Ba-123. That is, the apical oxygen is located in the middle of the Cu(1)-Cu(2) distance unlike Ba-123 where it is considerably displaced towards the Cu(1)-chains. The Sr-O bond lengths in the 1212 ($YSr_2Cu_2FeO_y$) and 1222 compounds are approximately equal for both the OS and OR samples. The effect of deoxygenation on the various bond lengths is the same as in Ba-123. The apical oxygen moves slightly towards the chains, while Sr moves closer to the Cu(2) planes.

Comparing the bond length Cu(2)-O(3) for both OS and OR with the Fe-O_{eq} and Cu-O_{eq} distances ($O_{eq} \equiv$ equatorial oxygen) in the $(Y,Ce)_2Sr_2CuFeO_8$ compound, we observe that the Fe-O_{eq} distance is almost equal to the Cu(2)-O(3) bond length while the Cu-O_{eq} distance is slightly larger ($\approx$ 0.05 Å).[3] For the comparison of the Cu(2)-O(2) bond length it is better to use the results of the OR 1222 sample. In any case the Cu(2)-O(2) bond length is among the Fe-O_{ax} and Cu-O_{ax} distances ($O_{ax} \equiv$ axial oxygen) of the $(Y,Ce)_2$ Sr_2CuFeO_8 compound, a fact that is expected since the Cu(2) sites are occupied simultaneously by Fe and Cu.

Bond valence sum calculations (see Table II) show that on Cu(2) resides a higher charge than on Cu(1) as in $Nd_2Ce_{0.67}Sr_{0.33}BaCu_3O_{9-y}$.[10] Contrary to this, in $YBa_2Cu_3O_{6.95}$ the valence of Cu(1) is larger than that of Cu(2).[11] As the oxygen content decreases the Cu(1) valence falls from 2 to 1.6 (as expected since the removal of oxygen reduces the chain copper neighbors), while that of Cu(2) decreases only slightly.

Finally, we discuss the oxygen environment of the Cu(1) and Cu(2) sites. Cu(1) is in disordered octahedral oxygen configuration and Cu(2) is fivefold coordinated. The various bond lengths with the surrounding oxygen atoms are nearly equal to those of the 1212 compound. This foretells us the similarity of the hyperfine parameters among the two 1212 and 1222 compounds (*vide infra*).

V. MAGNETIZATION MEASUREMENTS

Figure 4 shows the χ vs T curve of the OS sample for an applied field of 100 G. In the zero-field-cooling (ZFC) measurement it exhibits a peak at 24 K. This peak corresponds to a magnetic transition which comes either from long-range antifferomagnetic order or from a spin-glass transition. For further clarification neutron-scattering studies are needed. This T_{cusp} is lower than in the case of oxygenated YSr_2Cu_2 FeO_{6+y} where $T_{cusp} \approx 60$ K. The field-cooling data are similar to the ZFC except that for $T \leq 12$ K the susceptibility slightly increases. The data for $T > 25$ K were analyzed using the modified Curie-Weiss-type equation $\chi = C/(T - \Theta) + \chi_o$ where C is given by the relation:

$$C = \frac{\mu_{\text{eff}}^2 N}{3k_B}, \tag{1}$$

where N is the number of magnetic ions per unit volume, μ_{eff} is the effective magnetic moment, and k_B is the Boltzman constant. The parameters χ_o, C, and Θ are determined by a least-squares fit for the temperature range 25–300 K and for H=100 G. The effective magnetic moment is $\mu_{\text{eff}} = (1.9 \pm 0.1)\ \mu_B$ per ion and $\Theta = (-7 \pm 1)$ K. The negative value of Θ indicates antiferromagnetic correlations between the iron magnetic moments.

According to our Mössbauer results (*vide infra*) 56% of Fe is in the $S = 3/2$ state, 44% is in the $S = 5/2$ state. Therefore, assuming that Cu is in the $S = 1/2$ state, we should get $\mu_{\text{eff}} \simeq 3.2\ \mu_B$ per ion, a value that is nearly twice as large as the experimental one. This reduction of μ_{eff} may be due to the local antiferromagnetic exchange coupling between Fe and Cu moments. Therefore, μ_{eff} calculated from the above equation represents rather an

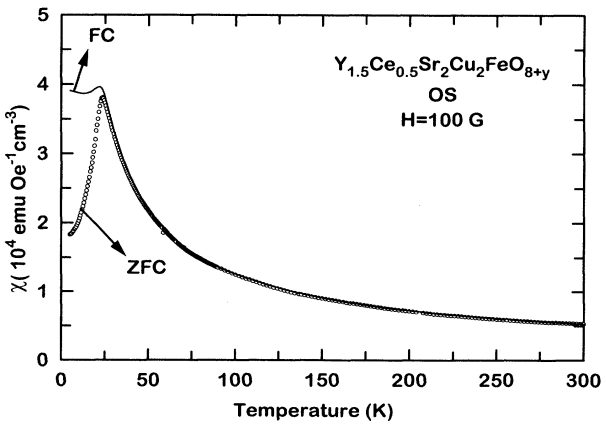

FIG. 4. Zero-field-cooled and field-cooled magnetic susceptibility vs temperature for the OS $Y_{1.5}Ce_{0.5}Sr_2Cu_2FeO_{8+y}$ sample in a magnetic field of 100 G.

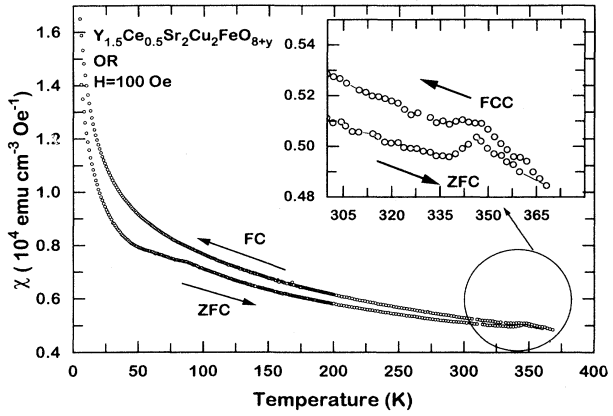

FIG. 5. Zero-field-cooled and field-cooled magnetic susceptibility vs temperature for the OR $Y_{1.5}Ce_{0.5}Sr_2Cu_2FeO_{8+y}$ sample in a magnetic field of 100 G.

apparent ion moment.

The magnetic-susceptibility curve for the reduced sample from 4.2 to 400 K is shown in Fig. 5. Around 350 K there is a distinct change of the slope as one can see in the inset of Fig. 5. Mössbauer spectroscopy revealed that for this sample a transition from paramagnetic to magnetic spectra occured at $T < 360$ K for the iron ions which occupy the Cu(2) sites. It is reasonable to attribute this anomaly to an antiferromagnetic transition of the Cu(2) sublattice. It is worth noting also an anomaly at about 80 K observed in the ZFC branch.

VI. MÖSSBAUER SPECTRA

The RT and 428 K ^{57}Fe Mössbauer spectra (MS) for the OS and OR $(Y,Ce)_2Sr_2Cu_2FeO_{8+y}$ samples are shown in Fig. 6, respectively. The results from the analysis of these spectra in two quadrupole doublets (denoted A_o, B_o for the OS sample and A_r, D_r for the OR sample) are summarized in Table III.

The spectrum of the OS sample does not display magnetic hyperfine splitting at 77 K and is similar to the RT spectrum. Above 350 K the OR sample is paramagnetic and can be fitted with the two doublets we mentioned in the first paragraph of this section. At $T \approx 360$ K the line shape of component A_r is broadened and for $T < 360$ K acquires a well resolved magnetic hyperfine structure. Regarding component D_r, it displayed a paramagnetic spectrum at RT (Fig. 7) and a very broad magnetic (or relaxed) spectrum at 77 K. The transitions observed in the MS of the OR sample are in agreement with the anomalies observed in the slope of the magnetic moment vs temperature curve.

The 4.2 K MS for both the OS and OR samples are shown in Fig. 8 and consist of two magnetic hyperfine sextets, as it is expected from the analysis of the corresponding MS in paramagnetic regime. The spectral lines are broadened with respect to the calibration linewidths, especially those of the components with the lower hyperfine magnetic field. Another feature is the selective broadening of the outer lines with respect to the inner lines. Possible causes for this broadening are spin fluctuations or a hyperfine field distribution due to inequivalent iron environment. In order to take the observed inhomogeneous broadening into account we fitted the spectra

TABLE III. Experimental values of the half linewidth $\Gamma/2$ in mm/s, the isomer shift δ relative to metallic Fe at RT in mm/s, the quadrupole shift ε in mm/s, the hyperfine magnetic field H in kG, the HWHM ΔH of the hyperfine magnetic field Lorentzian distribution which modulates the linewidths, as obtained from least-squares fits of the Mössbauer spectra. ε denotes the eigenvalues of the Hamiltonian of the quadrupole interaction or of the quadrupole pertrubation and are given by $\varepsilon = (1/4)e^2qQ(1+\eta^2/3)^{1/2}$, $\varepsilon = (1/8)e^2qQ(3\cos^2\theta - 1 + \eta\sin^2\theta\cos 2\phi)$ for the paramagnetic and the magnetic spectra, respectively. W is the relative intensity. The numbers in parentheses are estimated standard deviations referred to the last significant digit.

Sample	T	Site	$\Gamma/2$	δ	ε	H	ΔH	W%
	RT	A_o[a]	0.197(2)	0.280(1)	0.313(1)			44(1)
(OS)		B_o [b]	0.242(2)	-0.032(2)	0.394(1)			56(1)
	4.2 K	A_o	0.149(6)	0.384(3)	-0.131(3)	485(1)	13(1)	43(3)
(OS)		B_o	0.186(8)	0.058(8)	0.121(1)	258(1)	40(1)	57(3)
	428 K	A_r	0.229(5)	0.181(3)	0.379(3)			47(1)
(OR)		D_r[c]	0.206(4)	0.050(2)	0.850(2)			53(1)
	4.2 K	A_r	0.202(4)	0.404(2)	-0.166(2)	519(1)	3(1)	44(2)
(OR)		D_r	0.217(5)	0.272(4)	-3.714[d]	368(4)	64(4)	55(2)

[a] A_o and A_r represent Fe^{3+} ($S = 5/2$) at the Cu(2) sites.

[b] B_o represent Fe^{3+} ($S = 3/2$) or Fe^{4+} in distorted octahedral or pyramidal coordination at the Cu(1) sites.

[c] D_r represents Fe^{3+} ($S = 5/2$) in distorted tetrahedral coordination at the Cu(1) sites.

[d] This parameter is equal to eQV_{zz}. The angle θ and the asymmetry parameter η are estimated to be 90^0 and 0.05, respectively, by using the complete interaction Hamiltonian.

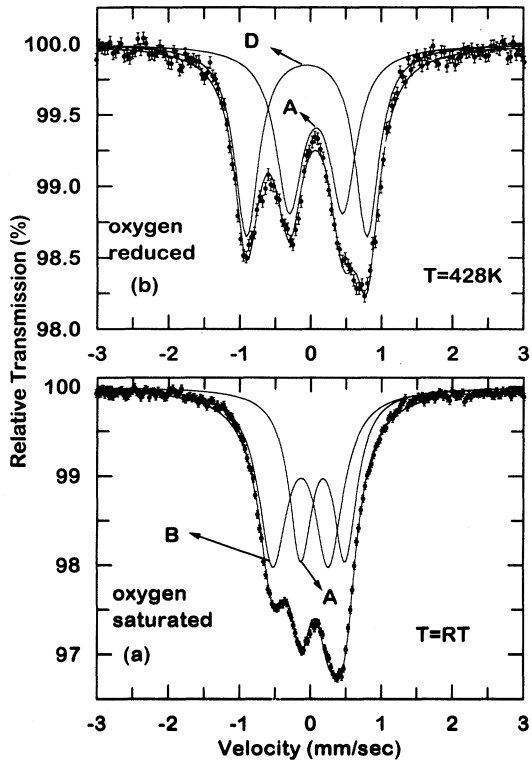

FIG. 6. Mössbauer spectra of $Y_{1.5}Ce_{0.5}Sr_2Cu_2FeO_{8+y}$ for (a) the OS sample at RT and (b) the OR sample at 428 K.

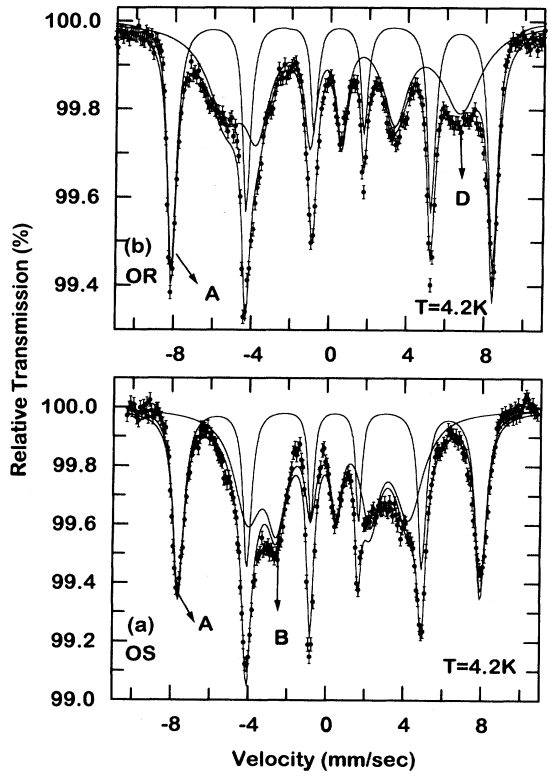

FIG. 8. 4.2 K Mössbauer spectra of $Y_{1.5}Ce_{0.5}Sr_2Cu_2FeO_{8+y}$ for (a) the OS sample and (b) the OR sample.

with Lorenzian lines, assuming that the hyperfine magnetic field follows a Lorentzian distribution. It is also worth noting that for the second sextet the assumption that the quadrupole energy is a first-order perturbation to the magnetic energy was proved to be inappropriate, since the theoretical spectrum could not describe satisfactorily the inner lines (3,4) of the sextet. Therefore, we had to use numerical diagonalization of the full Hamiltonian in order to obtain the hyperfine parameters for this component. The results from the fitting of the MS for the OS and OR sample at 4.2 K are summarized in Table III.

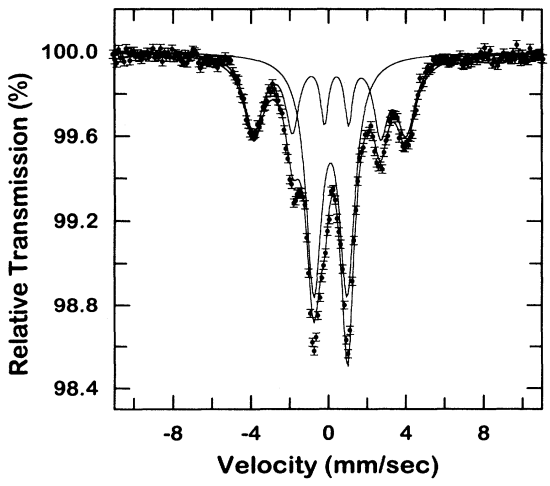

FIG. 7. Mössbauer spectra of OR $Y_{1.5}Ce_{0.5}Sr_2Cu_2FeO_{8+y}$ sample at RT.

In the following we will try to assign the observed Mössbauer components to certain distinct crystallographic sites. We start with the oxygenated sample. From the variation of the isomer shift with temperature, doublet A_o at RT has to be related to the 4.2 K magnetically splitted sextet with $H_{\text{eff}} = 485$ kG. This value of the hyperfine magnetic field implies Fe^{3+} at $S = 5/2$, although it is lower than the expected value of ≈ 520 kG. The observed value is lower either because $\langle S \rangle$ has not reached saturation or due to covalency phenomena between Fe and the neighboring oxygen ions. Based on the insensitivity of this component to the removal of oxygen [which occurs at the Cu(1) layers] and on the assignment we did in the case of $YSr_2Cu_{3-x}Fe_xO_y$,[12] it is reasonable to attribute this component to Fe located at the Cu(2) sites, in a square pyramidal coordination. Assigning this component to the Cu(2) sites, for which the principal axis of the electric-field gradient tensor is along the c axis and $\eta = 0$ (due to the tetragonal point symmetry) we can calculate the angle between the iron magnetic moment and the c axis from values of ϵ at RT and 4.2 K. Assuming that $q = V_{zz}/e$ is positive (as the calculation of V_{zz} using point charge approximation shows), the angle between $\langle S \rangle$ and the c axis is $\theta = 71° \pm 1°$. We should mention that the val-

ues of the isomer shift at RT and 4.2 K and of H_{eff} at 4.2 K were very close to the values obtained in the Mössbauer spectra of the $(Y,Ce)_2Sr_2CuFeO_8$ compound[3] where Fe occupies a site with square pyramidal coordination. Similar values for the hyperfine parameters mentioned above are also observed for iron which replaces Cu in the pyramidal site of isostructural $Eu_{1.5}Ce_{0.5}Sr_2NbCu_2O_{10}$,[5] or in $La_2CaCu_2O_6$ compounds.[13]

Component B_o for the OS sample has hyperfine parameters close to the parameters of component B that occurs in oxygen saturated $YSr_2Cu_{3-x}Fe_xO_y$ compounds.[12] Therefore, in analogy with this compound we assign it to Fe^{3+} ($S = 3/2$) which is located at the Cu(1) sites. At this point it is interesting to note that this assignment is not unique. This component can also be attributed to Fe^{4+} ($S = 2$). Typical values for Fe^{4+} ($S = 2$) in octahedral coordination are $\delta(\text{RT}) = 0.05$ mm/s, $\delta(\text{LHe}) = 0.15$ mm/s, and $H_{\text{eff}}(0) = 290$ kG (for $SrFeO_3$ compound).[14]

For the OR sample component A_r is related to the component with the large hyperfine magnetic field at 4.2 K. Following the same arguments as with the OS sample we can unambiguously assign this component to Fe^{3+} ($S = 5/2$) located at the Cu(2) sites. As we have already mentioned these sites are insensitive (except for the temperature where magnetic ordering takes place) to the amount of the oxygen contained in the Cu(1) layers. From the values of ϵ at 428 and 4.2 K we calculated the angle between the iron magnetic moment and the c axis to be $\theta = 70° \pm 1°$.

Since component A is present in both OS and OR samples we are led to the conclusion that sites B_o and D_r are complementary to each other with respect to the oxygen content. The behavior of components B_o and D_r is similar to the behavior of components C and A that occur in $YBa_2Cu_{3-x}Fe_xO_{6+y}$ with respect to the oxygen content[15] (note the different notation). Two recent works[16,17] in $YSr_2Cu_2Ga_{1-x}Fe_xO_7$ compound ($0 \leq x \leq 1$) for both reduced and oxygenated samples revealed the presence of a component with hyperfine parameters close to these of D_r. In this compound gallium exhibits a distorted tetrahedral coordination and is slightly displaced from the ideal Cu(1) sites of the 123 structure. In analogy with $YSr_2Cu_2Ga_{1-x}Fe_xO_7$ and $YSr_2Cu_{3-x}Fe_xO_y$ we can assign component D_r of the OR sample to Fe^{+3} located at the Cu(1) sites in a fourfold-distorted tetrahedral coordination. The same component is present in $YSr_2Cu_{2-x}Fe_xO_y$ for small values of x.[12] Based on the above interpretation for the D_r component, upon removing oxygen from the Cu(1) layers, the iron environment is changed in a coordination very close to that of Ga in the $YSr_2Cu_2GaO_8$ compound.[18]

Early studies of strontium ferrate $Sr_2Fe_2O_5$[14] and $Sr_2LaFe_3O_8$,[19] where both octahedral and tetrahedral Fe^{3+} ($S = 5/2$) ions are present, gave isomer shift values for the tetrahedral sites ≈ 0.17 mm/s (RT) and ≈ 0.28 mm/s (4.2 K), that are very close to the corresponding values of component D_r. However, the 4.2 K value of the hyperfine field for D_r is 370 kG that is 70–90 kG lower than the 4.2 K values for the tetrahedral sites in $Sr_2Fe_2O_5$ and $Sr_2LaFe_3O_8$. On the other hand, it is comparable to the 338 kG value observed[17] in an oxygen depleted $YSr_2Cu_2Fe_{0.8}Ga_{0.2}O_7$ sample. A possible explanation for this reduction of $H_{\text{eff}}(0)$ for component D_r is the dilution of the Cu(1) sublattice with nonmagnetic Cu^{1+} ions.

VII. RAMAN STUDY

The primitive cell of the 1222 structure contains 17 atoms [if we consider that the occupancy of O(1) is 1]. The atomic site symmetries and the corresponding Γ-point phonon modes are shown in Table IV.[20] From the in total 34 modes, two ($A_{2u} + E_u$) are acoustical, one (B_{2u}) is silent, 17 ($8A_{2u} + 9E_u$) are infrared active, and 14 ($5A_{1g} + 2B_{1g} + 7E_g$) are Raman active. The A_{1g} and B_{1g} modes correspond to atomic motions along the z direction, whereas the E_g modes are vibrations within the xy planes. The A_{1g} modes are allowed for xx, yy, zz but forbidden for crossed xy, zx, and zy polarizations of the incident and scattered radiation. The B_{1g} modes are allowed for the xx, yy, $x'y'$ but forbidden in the parallel zz $x'x'$ and crossed xy, zx, and zy configurations. The E_g modes are allowed in crossed zx and zy but forbidden for xy, $x'y'$, and all exact parallel configurations. Figures 9 and 10 show the zz and xx polarized spectra from zx-oriented microcrystal surfaces for the oxygenated and reduced samples, respectively. In zz polarization only the A_{1g} symmetry modes are allowed.

TABLE IV. Wyckoff notations, site symmetries, and irreducible representations for the atoms in $(Y,Ce)_2Sr_2Cu_2FeO_{8+y}$, space group $I4/mmm$.

Atom	Wyckoff notation	Site symmetry	Irreducible representations
Sr	4e	C_{4v}	$A_{1g} + A_{2u} + E_g + E_u$
Y	4e	C_{4v}	$A_{1g} + A_{2u} + E_g + E_u$
Cu(1)	2a	D_{4h}	$A_{2u} + E_u$
Cu(2)	4e	C_{4v}	$A_{1g} + A_{2u} + E_g + E_u$
O(1)	4c	D_{2h}	$A_{2u} + B_{2u} + 2E_u$
O(2)	4e	C^v_{4v}	$A_{1g} + A_{2u} + E_g + E_u$
O(3)	8g	C^v_{2v}	$A_{1g} + A_{2u} + B_{1g} + B_{2u} + 2E_g + 2E_u$
O(4)	4d	D_{2d}	$A_{2u} + B_{1g} + E_g + E_u$

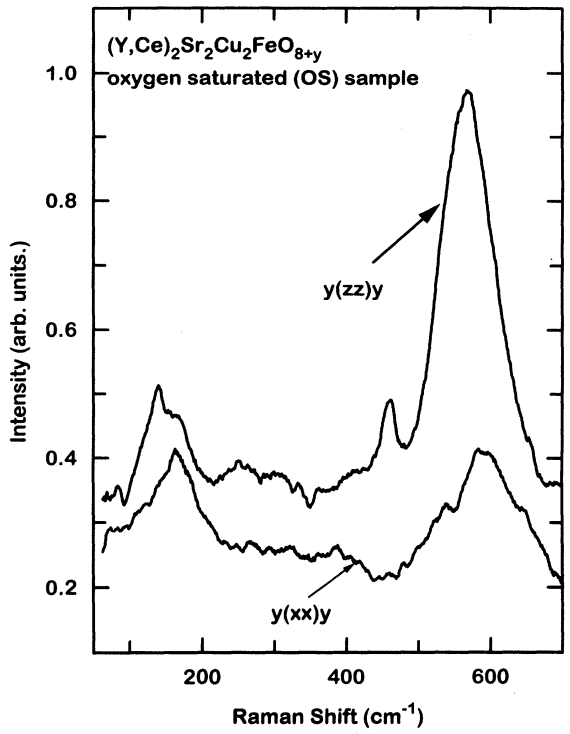

FIG. 9. zz and xx polarized Raman spectra of the $Y_{1.5}Ce_{0.5}Sr_2Cu_2FeO_{8+y}$ OS sample.

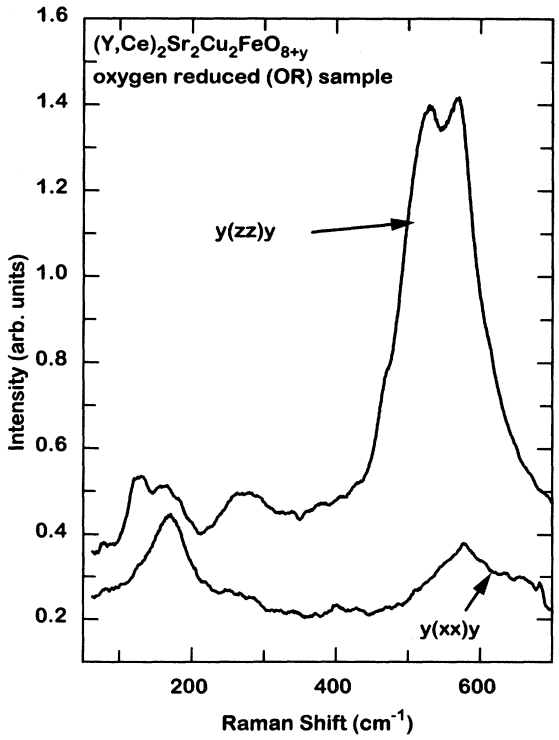

FIG. 10. zz and xx polarized Raman spectra of the $Y_{1.5}Ce_{0.5}Sr_2Cu_2FeO_{8+y}$ OR sample.

We start the assignment of the Raman lines from the ones at 136 and 122 cm^{-1} for the OS and OR samples, respectively. It is reasonable to assign this line to the A_{1g} mode involving mainly Cu(2) motion along the z axis. The softening of this mode in the OR sample can be attributed to the increase of the Cu(2)-O(2) bond length. The same mode has also been observed in compounds with similar structure. In $YBa_2Cu_3O_{6+y}$ this line occurs at 145 and 154 cm^{-1} for y =0.5 and $y \approx 2$, respectively.[21] Similarly, in $YBa_2Cu_4O_8$ and $YBa_2Cu_{4-x}Fe_xO_8$ this line occurs at about 153 cm^{-1}.[22,23] In compounds where Ba has been substituted with Sr, the bond lengths between Cu(2) and the nearest oxygen atoms are nearly equal to those of $(Y,Ce)_2Sr_2Cu_2FeO_{8+y}$. This mode occurs at 141 cm^{-1} in $YSr_2Cu_2GaO_7$,[24] and at 131 cm^{-1} in $(Y,Ce)_2Sr_2Cu_2(Cu,Bi)O_{9-y}$.[25] Finally, in $YSr_2Cu_{3-x}Fe_xO_y$ this mode occurs at 155 cm^{-1} with the A_{1g} mode of the Sr vibration along the z axis.[26]

By analogy to the above case we assign the mode at 165 cm^{-1} for OR and 160 cm^{-1} for OS sample to the A_{1g} vibration of Sr atom along the z axis. In $YBa_2Fe_3O_8$ (Ref. 27) and $YBaCuFeO_5$ (Ref. 28) the A_{1g} mode of Fe(2) occurs at 219 and 214 cm^{-1}, respectively. The above frequencies are considerably greater than those of $(Y,Ce)_2Sr_2Cu_2FeO_{8+y}$. Two can be the reasons for the hardening of this A_{1g} mode. The first is the smaller mass of Fe with respect to that of Cu and the second is the decrease of the bond length of Fe with the nearest oxygen atoms. Utilizing the Mössbauer results, 78% of the Cu(2) sites are occupied with Cu and 22% with Fe. The change of the frequency due to the mass change caused by the Fe substitution at the Cu(2) sites is approximately 1% or ≈ 2 cm^{-1}. This change is very small and therefore we cannot correlate the observed changes in the vibration frequency with the substitution of Fe at the Cu(2) sites.

In the 1222 structure there are two B_{1g} modes: one arising from the out-of-phase vibrations of the O(3) atoms and another arising from the out-of-phase vibrations of the O(4) atoms. In the structures where only the one B_{1g} mode is present (e.g., 123 compound) and related to the O(2) and O(3) vibrations, the frequency varies between 270 and 350 cm^{-1}. For compounds with a single B_{1g} mode involving out-of-phase vibrations of the oxygen atoms in the R-O layers (e.g., Nd_2CuO_4) the frequency varies between 297 and 347 cm^{-1}. As follows from Figs. 9 and 10 it is very probable that one line with B_{1g} symmetry has been observed at 165 cm^{-1} for the oxygenated and at 168 cm^{-1} for the reduced sample in the xx polarized spectra. Our results are comparable with these of Yoshida[29] in $(Eu_{2/3}Ce_{1/3})_2(Ba_{2/3}Eu_{1/3})_2Cu_3O_{8+y}$ where the low-frequency B_{1g} phonon has been observed at 180 cm^{-1}. As in our case the high-frequency B_{1g} mode is not observed due to its low intensity.

We assign the broad zz polarized structure at 261–318 cm^{-1} for the OS sample and at 273 cm^{-1} for the OR sample to the A_{1g} vibrations of Y and Ce atoms. The complex line shape of this band is an indication of a two-mode behavior. Alternatively, it may arise from the superposition of the (Y,Ce) A_{1g} Raman line and otherwise forbidden lines are activated by the substitution-induced

disorder.

The line that occurs at 460 cm^{-1} (OS) and at 469 cm^{-1} (OR) in the zz polarization can tentatively be assigned to the in-phase vibrations of the O(3) atoms in analogy with the 123 samples.[21] The strongest Raman band of A_{1g} symmetry is observed in the range 450–700 cm^{-1} for both samples. For the OS sample this band is a superposition of at least two Lorentzians centered at $\omega^{I} = 544$ cm^{-1} and $\omega^{II} = 514$ cm^{-1} with full width at half maximum (FWHM) $\Gamma^{I} \approx 44$ cm^{-1} and $\Gamma^{II} \approx 81$ cm^{-1}, respectively. In the OR sample this band is a superposition of at least three Lorentzians. The first occurs at $\omega[O(3)] = 469$ cm^{-1} and has already been attributed to the in-phase vibrations of O(3) along the z axis. The remaining two Lorentzians are centered at $\omega^{I} = 516$ cm^{-1} and $\omega^{II} = 516$ cm^{-1} with FWHM $\Gamma^{I} \approx 66$ cm^{-1}, and $\Gamma^{II} \approx 76$ cm^{-1}, respectively. One probable explanation is that the mode at 544 cm^{-1} for the OS sample and at 516 cm^{-1} for the OR sample corresponds to the A_{1g} c-axis motion of O(2). The mode at 576 cm^{-1} for the OS sample and at 569 cm^{-1} for the OR sample come from structural distortions and disordering effects.[30,31]

As we concluded from the analysis of MS especially from the OR sample, iron at Cu(1) sites has distorted tetrahedral coordination, a fact that necessarily leads to the shift of the ions at Cu(1) planes from the sites which space group $I/4mmm$ allows. So the vibrations of the oxygen ions at Cu(1) planes become Raman active.

Mode II has been observed in the same frequency range for the $(Y,Ce)_2Sr_2Cu_2(Cu,Bi)O_{9-y}$,[25] (583 cm^{-1}) and the $(Eu_{2/3}Ce_{1/3})_2(Ba_{2/3}Eu_{1/3})_2Cu_3O_{8+y}$,[29] (543 cm^{-1}) compounds and in lower range for the $YBa_2Cu_{3-x}Fe_xO_7$ (480–505 cm^{-1}) compound. It is worth noting that a similar band exists in the same frequency range for oxygenated $YSr_2Cu_{3-x}Fe_xO_y$,[26] and consists of two components at 535 and 565 cm^{-1}. As for the mode at 565 cm^{-1} it might come from structural distortions and disordering effects similar to the $Y_{1.5}Ce_{0.5}Sr_2Cu_2FeO_{8+y}$ compound.

VIII. DISCUSSION

We have studied the 1222 compound with three different techniques: x-ray powder diffraction, Mössbauer spectroscopy, and Raman spectroscopy. The x-ray diffraction patterns for both the OS and OR samples can be described with the average structural model presented in Table I, although we are dealing with a compound that has a great number of structural defects (deficient sites and cation disordering). The proposed model must be considered valid because the intensity of the diffraction peaks comes from an average unit cell.

In contrast to the x-ray powder diffraction which is a global probe since it gives information about the average structure to an extent of the order of 1 μm, Mössbauer and Raman spectroscopies are local probes. As it has been presented in the Mössbauer section, the existence of structural defects and oxygen deficient sites is clearly shown through the appearance of several Fe(1) components. The Mössbauer spectra also show that the strong local lattice distortion due to the substitution of Fe at the Cu(1) sites together with the deficiency of the O(1) site lead the trivalent iron atom to a ground state with a total spin less than the usual 5/2. The presence of large structural defects does not change the magnetic properties of the Cu(2) sublattice appreciably as shown from the Mössbauer spectra. For the OR sample, the Cu(2) sites show antiferromagnetic (AF) order as in the 123 compound. The degree of the disorder is also reflected in the broadening of the spectral lines. Consequently, in order to interpret the magnetic component of the OR sample we had to introduce the phenomenological parameter ΔH.

Mössbauer spectroscopy showed that Fe is equally distributed among the Cu(1) and Cu(2) sites. For small amounts of Fe, e.g., in the YBa_2Cu_{3-x} Fe_xO_{6+y} compound, Fe goes to the Cu(1) sites. A possible explanation is that the Fe atoms arrange themselves at the Cu(1) sites in such a way as to minimize the free energy of the system mainly through the decrease of the electrostatic energy. When the Fe doping exceeds a certain limit, as in $Y_{1.5}Ce_{0.5}Sr_2Cu_2FeO_{8+y}$, it is energetically favorable that a part of Fe goes to the Cu(2) sites. Probably, if all the Fe atoms were located at the Cu(1) sites then due to the large local structural distortions the increase in the free energy (mainly of electrostatic origin) would exceed the increase in the free energy due to the Fe substitution at the Cu(2) sites.

The Raman spectra reveal the disorder in a local scale unambiguously through the existence of bands instead of sharp peaks. It is worth noting that the large degree of defects, especially in the OR sample, leads to the presence of additional modes that are not allowed from the average structure.

In the Mössbauer spectra of the OR sample component B transforms into D which is attributed to Fe with fourfold-distorted tetrahedral coordination. In order to create such a coordination the oxygen atoms or even the Fe atoms must be displaced from their average structure positions to more asymmetric sites. This is reflected in the Raman spectra of the OR sample through the presence of additional peaks — that are otherwise not allowed by symmetry — in the band from 500 to 700 cm^{-1}. The centroids of the Raman bands and their variation with oxygen content follow the behavior observed in compounds with similar structure. Therefore, we suggest that the average properties follow the expected trends.

Regarding the magnetic properties it is worth comparing the present data with those of the isostructural OS $Pr_{1.5}Ce_{0.5}Sr_2Cu_2NbO_{10}$, $Eu_{1.5}Ce_{0.5}Sr_2Cu_2NbO_{10}$, and $Pr_{1.5}Ce_{0.5}Sr_2Cu_2GaO_9$ compounds.[5,32] While the first and the third compound display AF ordering at $\approx$ 100 K, the Eu counterpart, which is a superconductor, remains paramagnetic down to 4.2 K, and the $Y_{1.5}Ce_{0.5}Sr_2Cu_2FeO_9$ compound we examine in this work shows AF ordering at 24 K. There are two possible explanations for this difference. Either the (Pr,Ce) fluorite block affects the exchange coupling of the Cu (and Fe) moments in a different way than the (Eu,Ce) and (Y,Ce) blocks or (in the case of the Y) the large amount of Fe

creates some frustration in the Fe moments thus reducing the T_N.

Finally, it is worth noting that the presence of Fe leads to the stabilization of $Y_{1.5}Ce_{0.5}Sr_2Cu_2FeO_y$ in ambient oxygen pressure. However, the price for this stabilization is the creation of a large number of local defects and distortions. Therefore, the presence of many cations in a structure on the one hand results in the stabilization of the structure but on the other hand the minimization of the free energy is obtained through the appearance of large disordering effects. All the high-T_c superconductors that are stabilized through cation replacement show degraded superconductive properties. The absence of superconductivity in the present compound can be explained either with the substitution-induced disorder caused from Fe or with a combination of magnetic impurity scattering [there is 25% Fe substitution of Cu in the Cu(2)-O planes] and hole filling.

IX. CONCLUSIONS

We have prepared and characterized single phase $Y_{1.5}Ce_{0.5}Sr_2Cu_2FeO_{8+y}$. The structure was refined using the $I4/mmm$ space group. The Mössbauer data can be analyzed with three components as in the $YSr_2Cu_{3-x}Fe_xO_y$ phase. Component A is attributed to Fe^{3+} ($S = 5/2$) located in the Cu(2) planes and is present in all samples regardless of the preparation procedure. Component B is attributed to Fe^{3+} ($S = 3/2$) located in the Cu(1) site and is present only in the oxygen saturated sample. For the reduced and as prepared samples component B transforms into D which originates from Fe^{+3} ($S = 5/2$ or $S = 3/2$) in the Cu(1) site but with lower coordination number with respect to the iron of component B. From polarized micro-Raman spectra all five A_{1g} and the one from two B_{1g} Raman modes expected for the 1222 compound were identified.

ACKNOWLEDGMENTS

Partial support for this work was provided by the E.C. through the CHRX-CT93-0116, B/E-CT91-472 projects and from the 89EK19 project of the Greek Ministry of Industry and Technology.

* Electronic address: pissas@cyclades.nrcps.ariadne-t.gr

[1] J. C. Bednorz and K. A. Müller, Z. Phys. B **64**, 189 (1986).
[2] T. Wada, A. Nare, A. Incinose, H. Yamauchi, and S. Tanaka, Physica C **192**, 181 (1992).
[3] M. Pissas, C. Mitros, D. Niarchos, A. Kostikas, A. Simopoulos, M. Abrashev, V. Hadjimitov, and M. Iliev, Phys. Rev. B **50,** 10 157 (1994).
[4] M. Pissas, G. Kallias, A. Simopoulos, A. Kostikas, and D. Niarchos, Phys. Rev. B **46**, 14 119 (1992); M. G. Smith, R. D. Taylor, and J. D. Thompson, Physica C **208**, 91 (1993).
[5] I. Felner, U. Yaron, U. Asaf, T. Kröner, and V. Breit, Phys. Rev. B **49**, 6903 (1994).
[6] G. Kallias, V. Psyharis, D. Niarchos, and M. Pissas, Physica C **174**, 316 (1991).
[7] A. M. Balagurov, F. Bouree, I. S. Lyubutin, and I. Mirebeau, Physica C **228**, 299 (1994).
[8] D. B. Wiles and R. A. Young, J. Appl. Crystallogr. **14**, 149 (1981).
[9] I. D. Brown and D. Altermatt, Acta Crystallogr. B **41**, 244 (1985).
[10] D. Kovatcheva, P. Strobel, B. Souletie, and A. H. Hewat, Physica C **174**, 280 (1991).
[11] R. J. Cava, A. H. Hewat, E. A. Hewat, B. Batlogg, M. Marezio, K. M. Rabe, J. J. Krajewski, W. F. Peck, Jr., and L. W. Rupp, Jr., Physica C **165**, 419 (1990).
[12] M. Pissas, G. Kallias, E. Moraitakis, D. Niarchos, and A. Simopoulos, Physica C **234,** 127 (1994); V. Terziev, R. Suryanarayanan, Mamidanna S. R. Rao, L. Ouhammou, O. Gorochov, and J. L. Dormann, Phys. Rev. B **48**, 13 037 (1993); M. G. Smith, J. B. Goodenough, R. D. Taylor, J. J. Neumeier, and J. O. Willis, Physica C **222**, 157 (1994); M. G. Smith, J. Chan, and J. B. Goodenough, *ibid.* **208**, 412 (1993).
[13] I. Felner, D. Hechel, E. R. Yacoby, G. Hilscher, T. Holubar, and G. Schaudy, Phys. Rev. B **47**, 12 190 (1993).
[14] P. K. Gallagher, J. B. MacChesney, and D. N. E. Buchanan, J. Chem. Phys. **41,** 2429 (1964).
[15] For a detailed discussion and additional references see, P. Boolchand and D. McDaniel, in *Studies on High-Temperature Superconductors*, edited by A. V. Narlikar (Nova Science, Commack, New York, 1990), Vol. 4, p. 143; E. Baggio-Saitovich, Hyperfine Interact. **66**, 231 (1991).
[16] A. Rykov, V. Caignaert, and B. Raveau, J. Solid State Chem. **109**, 295 (1994).
[17] A. Rykov, V. Caignaert, G. Van Tendeloo, J. M. Greneche, F. Studer, N. Nguyen, A. Ducouret, P. Bonville, and B. Raveau, J. Solid State Chem. **113,** 94 (1994).
[18] G. Roth, P. Adelmann, G. Heger, R. Knitter, and Th. Wolf, J. Phys. (France) I **1,** 721 (1991).
[19] P. D. Battle, T. C. Gibb, and S. Nixon, J. Solid State Chem. **79,** 86 (1989).
[20] D. L. Rausseau, R. P. Bauman, and S. P. S. Porto, J. Raman Spectrosc. **10**, 253 (1981).
[21] R. M. Macfarlane, H. J. Rosen, E. M. Engler, R. D. Jacowitz, and V. Y. Lee, Phys. Rev. B **38**, 284 (1990).
[22] E. T. Heyen, R. Liu, C. Thomsen, R. Kremer, M. Cardona, J. Karpinski, E. Kaldis, and S. Rusiecki, Phys. Rev. B **41**, 11 058 (1990).
[23] Y. K. Atanassova, C. Mitros, G. Nicolaides, D. Niarchos, V. G. Hadjiev, and E. Liarokapis, Physica C **235-240**, 1181

(1994).
[24] D. Salamon, R. Liu, M. V. Klein, D. A. Groenke, K. R. Poeppelmeier, D. Dabrowski, P. D. Han, and D. A. Payne, Phys. Rev. B **47**, 12 242 (1993).
[25] M. V. Abrashev, V. N. Hadjimitov, L. N. Bozukov, and M. N. Iliev, Solid State Commun. **93**, 563 (1994).
[26] N. Poulakis, E. Liarokapis, G. Kallias, and M. Pissas (unpublished).
[27] Y. K. Atanassova, V. G. Hadjiev, P. Karen, and A. Kjekshus, Phys. Rev. B **50**, 586 (1994).
[28] Y. K. Atanassova, V. N. Popov, G. G. Bogachev, M. N. Iliev, C. Mitros, V. Psycharis, and M. Pissas, Phys. Rev. B **47**, 15 201 (1993).
[29] M. Yoshida, S. Tajima, Y. Mizuo, T. Wada, A. Ichinose, Y. Yaegashi, N. Koshizuka, H. Yamauchi, and S. Tanaka, Phys. Rev. B **44**, 782 (1991).
[30] M. Iliev, Y. Atanassova, L. Bozukov, J. Tihov, V. G. Hadjiev, and E. Liarokapis, Physica C **191**, 419 (1992).
[31] M. Iliev, C. Thomsen, V. Hadjiev, and M. Cardona, Phys. Rev. B **47**, 12 341 (1993).
[32] I. Felner, D. Sprinzak, U. Asaf, and T. Kröner, Phys. Rev. B **51**, 3120 (1995).